AIAA JOURNAL
Vol. 32, No. 4, April 1994

Adaptive Finite Element Method for Thermal Flow Problems

Dominique Pelletier,* Jean-François Hétu† and Florin Ilinca‡
École Polytechnique de Montréal, Montréal, Quebec, H3C 3A7, Canada

This paper presents an adaptive finite element method based on remeshing to solve incompressible viscous flow problems including heat transfer effects by forced or free convection. Conjugate heat transfer problems are also considered. Solutions are obtained in primitive variables by an Uzawa algorithm using a highly accurate finite element approximation on unstructured grids. Two error estimators are presented and compared on problems with known analytical solutions. The methodology is then applied to a problem of practical interest and predictions are compared with experimental measurements and show very good agreement.

Nomenclature

c_p = specific heat
e = error
f = body force
$\boldsymbol{g}$ = gravity vector
h = element size
$J(\cdot)$ = energy functional
k = thermal conductivity
$\boldsymbol{n}$ = outward unit vector
p = pressure
q_s = heat source
T = temperature
$\boldsymbol{u}$ = velocity vector
w = test function
β = volume expansion coefficient
δ = element size for new mesh
ε = strainrate tensor
η = relative error
μ = viscosity
ρ = density
σ = stress tensor
∇ = gradient
$\nabla\cdot$ = divergence

Subscripts

av = average
∂, B = boundary
∞ = reference value

Introduction

ADAPTIVE finite element methods provide a powerful approach for tackling complex computational fluid dynamics problems. They provide a framework for optimizing several aspects of the computational process. For instance, grid points are clustered in regions of rapid solution variation to improve accuracy. This is done in such a way as to result in a uniformly accurate solution throughout the domain. The adaptive process is also cost effective in the sense that the best numerical solution is obtained at the least computational cost. Moreover, such approaches provide flexibility in modeling and algorithm development and can, at least in theory, provide quantitative measures of the accuracy of the solutions computed.

Initial breakthroughs were achieved in aerodynamics because of the pressing need for accurate computations of shockwaves.[1] However, little work has been done for incompressible flows and even less for thermal flow problems. Proof of concept computations were reported in Refs. 2 and 3. However these papers did not address the issue of quantitative assessment of the proposed methods. This paper presents an extension of the authors' previous work on adaptive remeshing to thermal flow problems.[4–6] The method is based on adaptive remeshing coupled to a finite element solver for steady-state incompressible flows including heat transfer effects.

The paper is organized as follows: First the equations of motion and the finite element solver are reviewed. The methodology section describes the two error estimators and the adaptive remeshing strategy. The methodology is validated on problems with known analytical solutions. The method is then applied to free convection in a square cavity and in a partially divided enclosure for which measurements are available. The paper closes with a conclusion.

Finite Element Solution Algorithm

Equations of Motion

The flow regime of interest is modeled by the Navier-Stokes equations with the Boussinesq approximation:

$$\rho \boldsymbol{u}\cdot\nabla\boldsymbol{u} = -\nabla p + \nabla\cdot\sigma + f - \rho\boldsymbol{g}\beta(T - T_\infty)$$

$$\nabla\cdot\boldsymbol{u} = 0$$

$$\rho c_p \boldsymbol{u}\cdot\nabla T = \nabla\cdot(k\nabla T) + 2\mu\varepsilon(\boldsymbol{u}) : \varepsilon(\boldsymbol{u}) + q_s$$

where the stress tensor σ, and the strainrate tensor ε are defined by

$$\sigma = 2\mu\varepsilon(\boldsymbol{u}) = \mu\{\nabla\boldsymbol{u} + (\nabla\boldsymbol{u})^T\}$$

Appropriate boundary conditions complete the statement of the problem

$$\boldsymbol{u} = \boldsymbol{u}_0 \quad \text{on } \Gamma_u$$
$$2\mu\varepsilon(\boldsymbol{u})\cdot\boldsymbol{n} - p\boldsymbol{n} = \hat{t} \quad \text{on } \Gamma_{\hat{t}}$$
$$T = T_0 \quad \text{on } \Gamma_T$$
$$k\nabla T\cdot\boldsymbol{n} = q_B \quad \text{on } \Gamma_q$$

Received Dec. 30, 1992; presented as Paper 93-0920 at the AIAA 31st Aerospace Sciences Meeting, Reno, NV, Jan. 11–14, 1993; revision received Aug. 18, 1993; accepted for publication Sept. 20, 1993.

*Associate Professor. Member AIAA.
†Graduate Research Assistant; currently Research Officer, National Research Council of Canada, Institute for Industrial Materials, 75 Montarville, Boucherville, Canada.
‡Graduate Research Assistant.

Finite Element Solver

The starting point for the finite element solver is the weak or Galerkin form of the equations of motion. The preceding equations are multiplied by an appropriate test function and diffusion terms are integrated by parts over the domain. The resulting variational form is given by:

$$(\rho \boldsymbol{u} \cdot \nabla \boldsymbol{u}, v) + a(\boldsymbol{u}, v) - (p, \nabla \cdot v) + (\rho g \beta T, v)$$

$$= (f, v) + (\rho g \beta T_\infty, v) + \langle \hat{t}, v \rangle$$

$$(q, \nabla \cdot \boldsymbol{u}) = 0$$

$$(\rho c_p \boldsymbol{u} \cdot \nabla T, w) + d(T, w) = (\tau : \varepsilon, w) + (q_s, w) + \langle q_B, w \rangle$$

with

$$a(\boldsymbol{u}, v) = \int_\Omega 2\mu \varepsilon(\boldsymbol{u}) : \varepsilon(v)\, d\Omega$$

$$d(T, w) = \int_\Omega k \nabla T \cdot \nabla w\, d\Omega$$

$$\langle \hat{t}, v \rangle = \int_{\partial K \setminus \Gamma_i} [2\mu \varepsilon(\boldsymbol{u}) \cdot \boldsymbol{n} - p\boldsymbol{n}] \cdot v\, ds + \int_{\partial K \cap \Gamma_i} \hat{t} \cdot v\, ds$$

$$\langle q_B, w \rangle = \int_{\partial K \setminus \Gamma_q} (k \nabla T) \cdot \boldsymbol{n} w\, ds = \int_{\partial K \cap \Gamma_q} q_B w\, ds$$

The seven-node Crouzeix-Raviart triangular element, with enriched quadratic velocity interpolation and discontinuous linear pressure approximation, is used to discretize the equations of motion (see Ref. 4). Temperature is approximated by quadratic polynomials. The pressure degrees of freedom are treated by an augmented Lagrangian formulation which eliminates pressure as a primary unknown. The only remaining unknowns are the velocity components and temperature. The finite element equations are assembled in a compacted skyline format and linearized with Newton's method. The resulting sparse linear system of equations is solved by Gaussian elimination.

Adaptive Methodology

Generalities

Most adaptive methods assess the quality of an initial solution obtained on a coarse mesh by using some form of error estimation and modify the structure of the numerical approximation in a systematic fashion to improve the overall quality of the solution. There are several ways of achieving adaptivity: *P* methods increase the degree of polynomial approximations for improved accuracy[7]; *R* methods relocate grid points in regions of rapid change of the solution,[8] and *H* methods proceed by either mesh enrichment or remeshing.[1,4]

A variant of an *H* method, called adaptive remeshing, has been retained because it provides the greatest control of element size and grading to accurately resolve flow features such as shear and thermal layers, stagnation points, jets, and wakes. In this approach the problem is first solved on a coarse grid to roughly capture the physics of the flow. The resulting solution is then analyzed to determine where more grid points are needed and an improved mesh is generated. The problem is solved again on the new mesh using the solution obtained on the coarser mesh as an initial guess. This process is repeated until the required level of accuracy is achieved.

Remeshing also offers an elegant and simple approach to overcome some of the obstacles specific to incompressible viscous flows. For instance, the best proven finite element approximations can be selected based on their convergence and accuracy properties.[9,10] This circumvents the problem associated with *P* methods of satisfying the so-called Ladyzhenskaya-Babuska-Brezzi (LBB) compatibility condition between the velocity and pressure approximations. It also eliminates the hanging node problem encountered in some *H* refinement methods.[3]

Error Estimation

This section describes two error estimation techniques for assessing the accuracy of the solutions obtained by the finite element solver.

Projection

This approach was first introduced by Zienkiewicz and Zhu[11] and involves post processing of the stresses and strains. For isothermal incompressible flows, this estimator can be derived from the variational principle for Stokes flow which consists in finding a velocity vector U which minimizes the dissipation energy:

$$J(U) = \int \frac{1}{2} \mu (U_{i,j} + U_{j,i}) : (U_{i,j} + U_{j,i})\, dv = \int \sigma : \varepsilon\, dx$$

If U_h and U_{ex} are the approximate and exact solutions, respectively, the dissipation energy of the error can be computed by evaluating

$$J(e) = J(U_h - U_{ex}) = \int (\sigma_h - \sigma_{ex}) : (\varepsilon_h - \varepsilon_{ex})\, dx$$

Unfortunately, the exact solution is not available in cases of practical interest. However, it has been shown that the exact stresses and strains can be replaced by a continuous least-squares approximation. See Ref. 12 for details. This estimator has proven useful because its sensitivity to high strains allows for automatic detection of boundary layers and stagnation points.[4,5]

This estimator does not include the effects of pressure and temperature. However, it is a simple matter to generalize the estimator to properly treat thermal problems. The pressure and temperature gradients being discontinuous, their least-squares projection into the space of velocity interpolation functions is easily computed. The pressure and temperature contributions to the error are given by

$$e_h^p = \tilde{p}_h - p_h$$

$$\frac{\partial e_h^T}{\partial x} = \frac{\partial \tilde{T}_h}{\partial x} - \frac{\partial T_h}{\partial x}$$

where the " ~ " denotes a least-squares projection.

The combined norm of the velocity, pressure, and temperature errors is then computed as follows:

$$\| (\boldsymbol{u}, p, T) \|_T = \left\{ \|\boldsymbol{u}\|_E^2 + \|p\|_0^2 + \int_\Omega k^2 \nabla T \cdot \nabla T \right\}^{1/2}$$

where

$$\|\boldsymbol{u}\|_E = \left\{ \int_\Omega 4\mu^2 \varepsilon(\boldsymbol{u}) : \varepsilon(\boldsymbol{u})\, d\Omega \right\}^{1/2}$$

$$\|p\|_0 = \left\{ \int_\Omega | p |^2\, d\Omega \right\}^{1/2}$$

Incorporation of pressure terms in the error estimator was shown to play a critical role in obtaining accurate predictions of reattachment point flows. For such cases velocity gradients are small and pressure variations control the flow.[5]

Local Partial Differential Equation Problem for the Error

This approach provides estimates of the error without having to solve the global least-squares problems required for the Zhu esti-

mator. Partial differential equations (PDE) and their weak forms for the velocity, pressure, and temperature errors can be derived directly from the Navier-Stokes equations[5,6,12]:

$$a(\boldsymbol{e}^{\boldsymbol{u}}, v) - (e^{p}, \nabla \cdot v) + (\rho \boldsymbol{g} \beta e^{T}, v) = -a(\boldsymbol{u}, v)$$

$$+ [f - \rho \boldsymbol{u}_h \cdot \nabla \boldsymbol{u}_h - \rho \boldsymbol{g} \beta (T_h - T_\infty), v_h] + (p_h, \nabla \cdot v_h)$$

$$+ \langle [2\mu\varepsilon \cdot \boldsymbol{n} - p_h \boldsymbol{n}]_A, v_h \rangle_{\partial k \setminus \Gamma_i} + \langle \hat{\boldsymbol{t}}, v_h \rangle_{\partial K \cap \Gamma_i}$$

$$(q_h, \nabla \cdot \boldsymbol{e}_h^{\boldsymbol{u}}) = (q, \nabla \cdot \boldsymbol{u}_h)$$

$$d(e_h^T, w_h) = (q_s - \rho c_p \boldsymbol{u}_h \cdot \nabla T_h + 2\mu\varepsilon : \varepsilon, w_h)$$

$$-d(T_h, w_h) + \langle q_B, w_h \rangle_{\partial K \cap \Gamma T} + \langle [k \nabla T_h \cdot \boldsymbol{n}]_A, w \rangle_{\partial k \setminus \Gamma_q}$$

The terms in parentheses on the right-hand sides represent the element residual, a measure of the accuracy of the finite element solution inside an element. The terms in brackets are the average momentum and heat fluxes across element faces. The difference between this average value and the raw fluxes computed on the face of the element reflects how well the solutions on two neighboring elements are matched. The second equation is a measure of mass conservation.

This variational problem is discretized locally on each element. Velocity and temperature errors are approximated with three quartic bubble functions associated to the midside nodes of the triangle. The pressure error is approximated with an appropriate bubble function. This results in small 10×10 systems of equations which are inexpensive to solve.[6] The norm of the combined errors is computed using the same norm used in the projection error estimate.

Adaptive Remeshing

There remains one key issue to discuss: how does one exploit the knowledge of the error distribution to design a better mesh? The adaptive remeshing strategy is straightforward and follows that proposed in Ref. 1, and proceeds as follows:

Step 1) Generate an initial mesh.
Step 2) Compute the finite element solution.
Step 3) Compute error estimate.
Step 4) If (global error < tolerance) then
- stop

else
- Compute grid density from error estimate
- Generate an improved mesh according to grid density
- Interpolate current solution on new mesh
- Go to Step 2

end if.

We now provide details on some of the steps of this algorithm.

Once the finite element solution has been obtained, the error on each element is computed using one of the previously described estimators. The global norms of the solution and the error are computed as follows

$$\|e_{\text{tot}}\|^2 = \sum \|e_k\|^2$$

so that the relative error can be evaluated.

$$\eta = \|e_{\text{tot}}\|^2 / \|U\|$$

There remains to compute the element size for the improved mesh so that elements are smaller in regions of large error and bigger in regions where the solution is already accurate. This is achieved by requiring that the improved mesh be optimal (i.e., that all elements have the same average error e_{av}). Now, given a target relative error η_t, the total and average error can be related as follows:

$$\|e_{\text{av}}\| = \eta_t \frac{\|U\|}{\sqrt{n}}$$

Finally, an expression for element sizes can be derived from the asymptotic rate of convergence of the finite element approximation which relates the error to some power k of the element size h:

$$\|e\| = ch^k$$

This can also be written for the target error:

$$\|e_{\text{av}}\| = c\delta^k$$

These two equations can be solved for the required element size:

$$\delta = \left[\frac{\tilde{\eta}_t \|U\|}{\|e\| \sqrt{n}}\right]^{1/k} h$$

which is then used as the grid density in the advancing front mesh generator to generate an improved mesh.

Validation

The two error estimators are first compared on simple flow problems for which an analytical solution is known. This provides controlled conditions to validate the proposed adaptive strategy and assess its computational performance.

One-Dimensional Thermal Boundary Layer

For this problem the analytical solution was taken to be:

$$u = 1 - y^2$$

$$v = 0$$

$$p = x$$

$$T = [\cosh(a) - \cosh(ay)]/[\cosh(a) - 1]$$

The constant a controls the thickness of the thermal boundary layer. In this problem only the temperature field will contribute to the error since the finite element approximation provides an exact representation of the velocity and pressure fields. The problem is solved on the unit square. The adaptive strategy is set to reduce the computed error by a factor of three at each cycle. Tables 1 and 2

Table 1 One-dimensional case, projection estimator

Mesh	Number of nodes	Number of elements	Error estimate	True error
0	347	106	0.03327	0.1070
1	587	187	0.009959	0.03079
2	1135	361	0.006189	0.01412
3	1589	514	0.003254	0.007732

Table 2 One-dimensional case, local problem estimator

Mesh	Number of nodes	Number of elements	Error estimate	True error
0	347	106	0.09737	0.1070
1	421	134	0.02924	0.04832
2	945	306	0.01264	0.01831

Table 3 Two-dimensional case, projection estimator

Mesh	Number of nodes	Number of elements	Error estimate	True error
0	89	36	0.006162	0.02435
1	226	101	0.004506	0.01507
2	647	300	0.002931	0.00644
3	1038	487	0.0009619	0.00258

Table 4 Two-dimensional case, local problem

Mesh	Number of nodes	Number of elements	Error estimate	True error
0	89	36	0.01734	0.02435
1	178	79	0.01472	0.02101
2	356	163	0.00478	0.01332
3	731	344	0.00258	0.00527

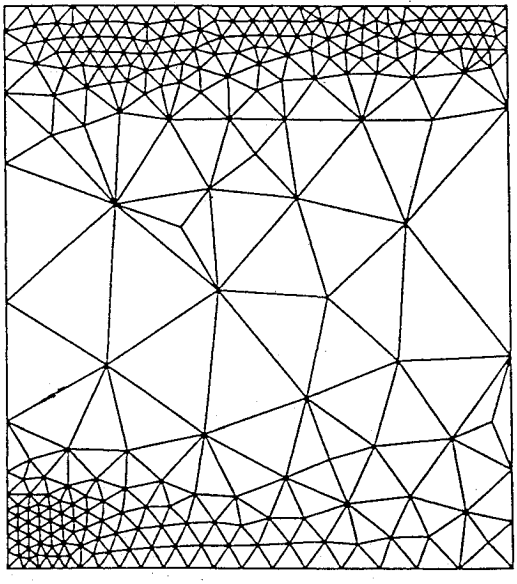

Fig. 1 Final mesh for two-dimensional boundary layer.

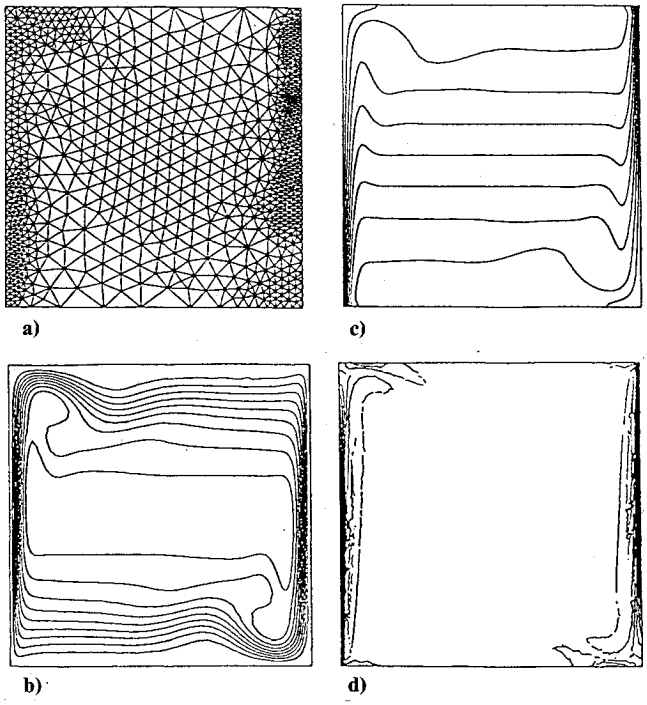

Fig. 2 Cavity: local problem approach: a) mesh, b) streamlines, c) temperature, and d) vorticity.

Table 5 Square cavity, projection estimator

Mesh	Number of nodes	Number of elements	Error estimate	Solution norm
0	701	320	0.0005358	0.1473
1	954	441	0.0003718	0.1477
2	2863	1368	0.0001094	0.1480

Table 6 Square cavity, local problem

Mesh	Number of nodes	Number of elements	Error estimate	Solution norm
0	701	320	0.0006204	0.1473
1	1047	490	0.0003536	0.1494
2	3647	1962	0.00009115	0.1480

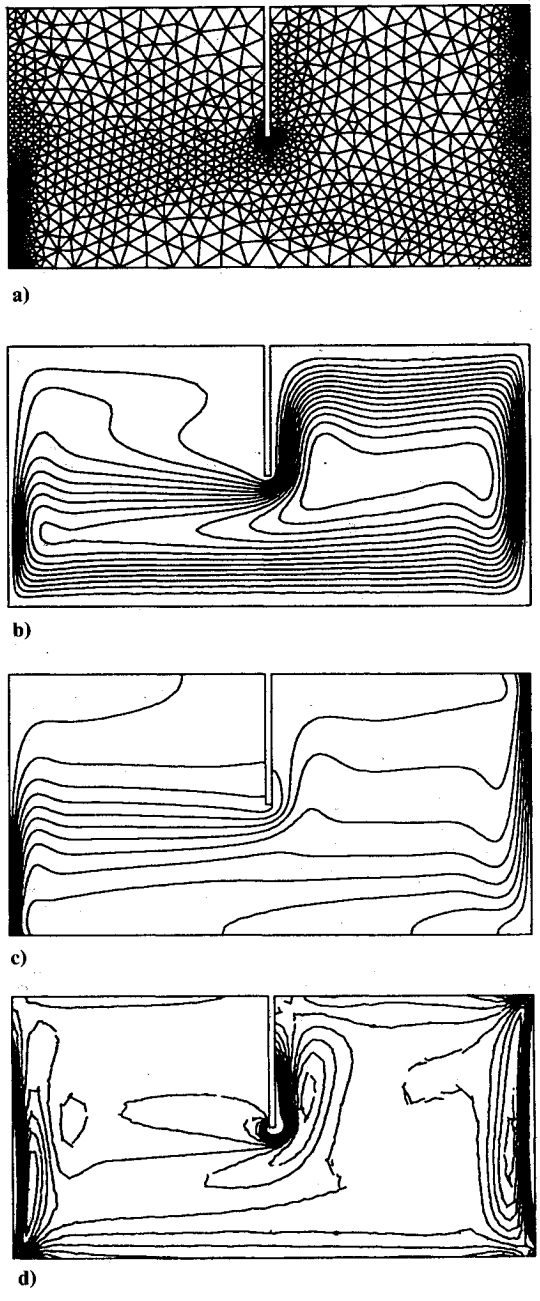

Fig. 3 Enclosure: a) mesh, b) streamlines, c) temperature, and d) vorticity.

illustrate the performance of the adaptive strategy for both the projection and local problem error estimators. As can be seen, both the true error and its estimate are reduced at each cycle.

Two-Dimensional Thermal Boundary Layer

A more realistic flow problem is obtained by taking

$$u = 1 - \exp(\xi)$$

$$p = x$$

$$\xi = y\,[U_0/(\nu x)]^{1/2}$$

$$T = [\cosh(a) - \cosh(ay)]/[\cosh(a) - 1]$$

The similarity variable ξ produces a velocity field that closely resembles that of a boundary layer on a flat plate. The temperature exhibits a thin thermal layer in the freestream. This test case retains many nonlinear terms present in the Navier-Stokes equations, thus providing a more stringent test for the error estimators. This problem offers a further challenge for the adaptive strategy because the error estimators should automatically detect the two boundary layers.

Tables 3 and 4 show that both error estimators drive the adaptation process to reduce the error at each cycle. Figure 1 illustrates the mesh designed by the projection method at the third cycle. One can clearly see that element sizes reflect the thickening of the hydrodynamic boundary layer on the bottom wall as one proceeds from left to right. The thermal boundary layer on the top of the domain is of constant thickness by design and one can see that the adaptive process produces a fairly uniform grid in that region.

In summary, the adaptive strategy performs well. Both error estimators ensure a reduction of the true error at each cycle so that the solution accuracy improves steadily at each adaptation cycle.

Applications

This section presents application of the error estimators to more complex problems. The adaptive strategy was set to attempt a reduction of the error by a factor of three at each cycle. The adaptive procedure is fully automatic and requires no user intervention. Both error estimators lead to very similar results. Hence, only one set of plots is presented for each problem.

Free Convection in a Square Enclosure

This is a classical test case for free convection. The top and bottom walls are adiabatic, the left one is hot and the right one is cold. Calculations were performed at a Rayleigh number of 10^7. Tables 5 and 6 show the behavior of the adaptive process with the projection and local problem estimators. As can be seen both estimators behave similarly initially. Error estimates, solution norms, and mesh characteristics are comparable. Differences appear in the mesh at the second cycle for which the local problem approach produces a somewhat more refined mesh.

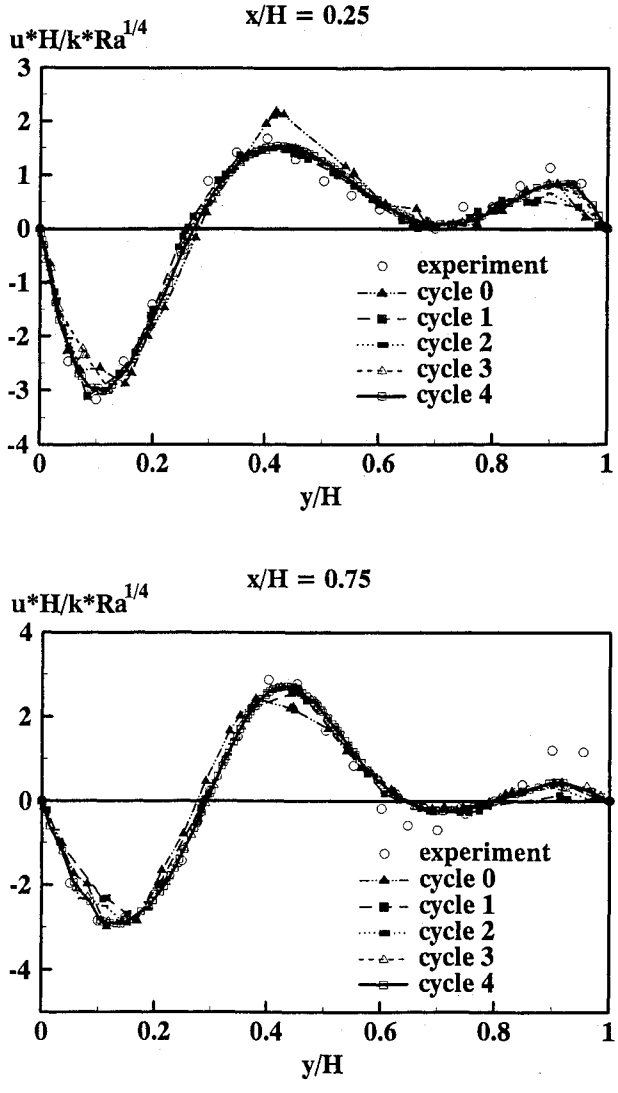

Fig. 4 Enclosure: velocity at x/h = 0.25 (top), velocity at x/h = 0.75 (bottom).

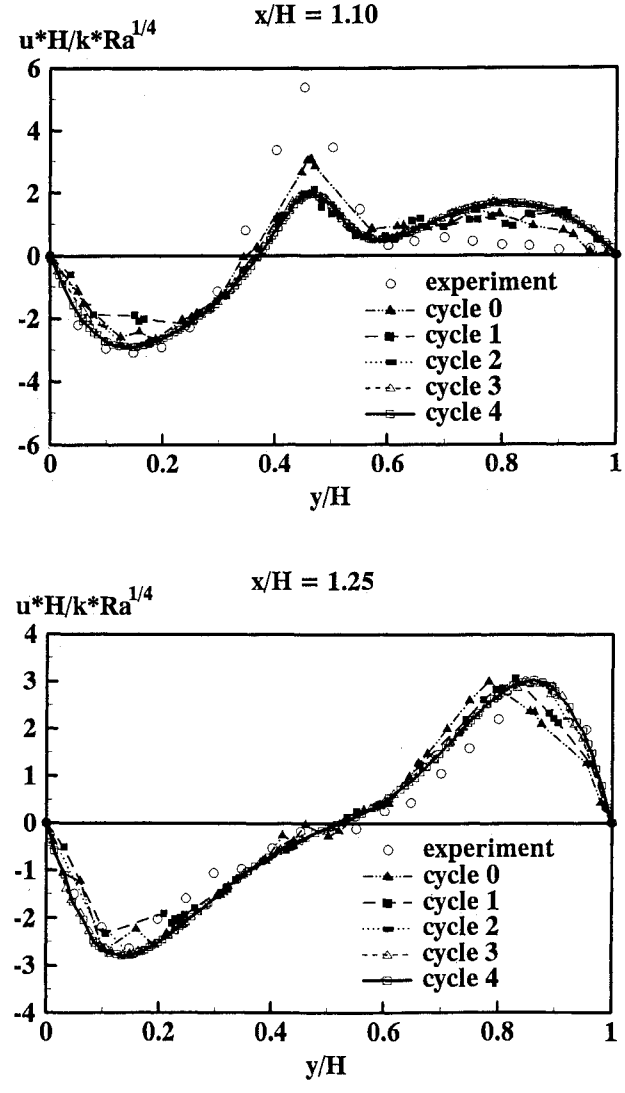

Fig. 5 Enclosure: velocity at x/h = 1.1 (top), velocity at x/h = 1.25 (bottom).

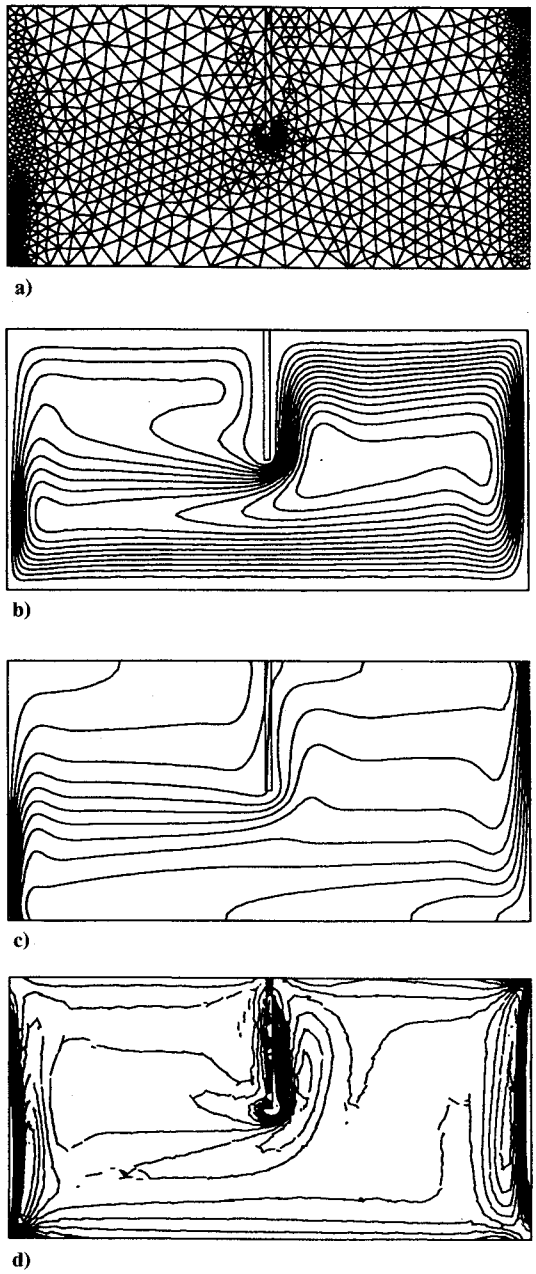

Fig. 6 Enclosure with conducting partitions a) mesh, b) streamlines, c) temperature, and d) vorticity.

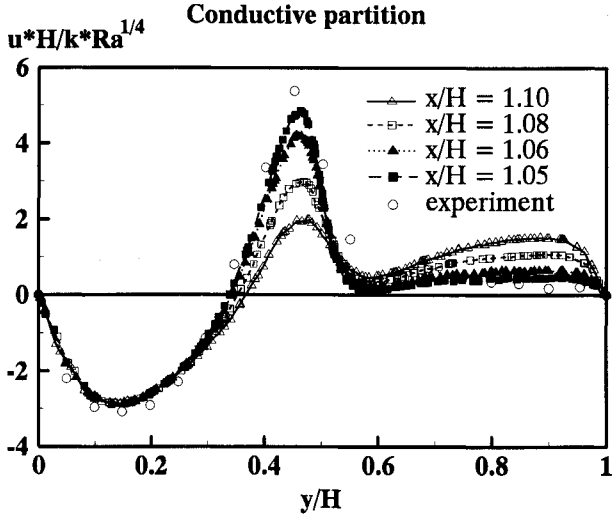

Fig. 7 Enclosure: jet predictions.

Figure 2 shows typical mesh, streamlines, isotherms, and vorticity contours obtained after the second cycle of adaptation. While vorticity is physically continuous, its values computed from the finite element approximation are discontinuous across element faces. As the mesh is adapted and refined the discontinuous vorticity contours should tend towards solid continuous lines. As can be seen from Fig. 2, vorticity contours are nearly continuous indicating that the adaptive process behaves properly. The mesh, streamlines, isotherms, and vorticity contours present a remarkable level of symmetry with respect to the center of the cavity, further confirming the physically realistic behavior of the proposed adaptive strategy. Finally, velocity and temperature profiles compare very well with the most reliable data available in the literature.

Free Convection in Partitioned Enclosure

This computation reproduces the experimental conditions of Chen et al.[13] The partition and the top and bottom walls are insulated. The left and right walls are maintained at a hot and cold temperature, respectively. Computations were performed at a Rayleigh number of 10^6 for which measurements are available. Note that it is assumed that the polyacrilate partition behaves as an adiabatic wall while in fact heat is conducted through the partition.

Figures 3 shows the final mesh, streamlines, isotherms, and vorticity contours obtained after three cycles of adaptation. As can be seen, grid points were clustered in the vertical boundary layers and around the partition corner where the fluid is highly accelerated.

Figures 4 and 5 compare predictions of axial velocity with the measurements of Chen along four vertical stations. As can be seen, predictions are in excellent agreement with measurements at $x/H = 0.25$, 0.75, and 1.25. At the $x/H = 1.1$ station, the predictions are good for the reverse flow on the bottom wall ($y/H < 0.25$). Predictions miss the high velocity peak near the tip of the partition and overpredict the velocity in the boundary layer along the top wall.

The simulation was redone to include heat conduction in the solid partition to determine if the adiabatic condition of the partition is responsible for the poor predictions of the jet near the tip of the partition. Figure 6 shows the mesh, streamlines, isotherms, and vorticity contours obtained after three cycles. One can clearly see differences in the streamlines and isotherms. However, comparison of velocity profiles with measurements did not show any drastic improvements. Modeling of conduction in the partition did not lead to any significant improvement in predictions at $x/H = 1.1$.

Finally, Fig. 7 compares predictions at $x/H = 1.06$ with measurements taken at $x/H = 1.1$. This stunning agreement could hint to uncertainty (3.5%) in the positioning of the traversing mechanism used for taking the velocity measurements. However, it is not possible to make a definite judgement because details of the experimental procedure are not available.

Discussion

Results from the preceeding section illustrate the accuracy improvements achieved through adaptivity. The proposed methods also results in a cost-effective solution algorithm that is well worth the added complexity. In Ref. 5 the authors have shown that, for isothermal flows, computation of the error estimate typically represents less than 8% of the cost of obtaining a solution on a given mesh. Timing data from Ref. 5 also indicates that the adaptive strategy offers a three- to fourfold reduction in CPU time when compared to solving the problem directly on the fine mesh. Similar results were obtained for the present class of flows, but space limitation does not allow for presentation of detailed timing data.

The reader may also wonder if there is any advantage in using one error estimator rather than the other. Numerical experiments indicate that the projection estimator is less expensive than the local problem approach except on coarse meshes. This can be explained by the fact that the least-squares matrix is nearly full on coarse meshes and that its sparsity increases with each cycle of refinement. Furthermore, the projection matrix is the same for all components of the diffusion fluxes. Hence the matrix can be factored once and for all and only forward and backward substitutions

need be performed for each projection. This makes the projection approach computationally more efficient than the local problem approach. Finally, its implementation is straightforward.

On the other hand, the local problem for the error is derived directly from the differential equations and boundary conditions. It embodies all of the mathematics and physics of the flow problem being solved. Thus, this approach is more general and capable of treating more complex problems and boundary conditions. This increased generality is achieved at the expense of a more intricate implementation. The error estimator is also slightly more expensive.

Conclusions

An adaptive remeshing finite element procedure has been presented for solving complex viscous flows including heat transfer effects by free or forced convection. The two proposed error estimators have been shown to be reliable and convergent by solving problems with known analytical solutions. The estimators are sensitive to both hydrodynamic and thermal layers. The proposed adaptive procedure has shown to be very robust. It can be used in a nearly blackbox fashion with little or no intervention on the part of the user. Finally, complex flows including heat conduction in immersed solid bodies can easily be treated with the proposed methodology.

References

[1]Peraire, J., Vahdati, M., Morgan, K., and Zienkiewicz, O. C., "Adaptive Remeshing for Compressible Flows," *Journal of Computational Physics*, Vol. 72, No. 2, 1987, pp. 26–37.

[2]Wu, J., Zhu, J. Z., Szmelter, J., and Zienkiwicz, O. C., "Error Estimation and Adaptivity in Navier-Stokes Incompressible Flows," *Computational Mechanics*, Vol. 6, No. 3, 1990, pp. 259–270.

[3]Wang, K. C., and Carey, G. F., "Adaptive Grids for Coupled Viscous Flow and Transport," *Computer Methods in Applied Mechanics and Engineering*, Vol. 82, No. 2, 1990, pp. 365–383.

[4]Hétu, J.-F., and Pelletier, D., "Adaptive Remeshing for Viscous Incompressible Flows," *AIAA Journal*, Vol. 30, No. 8, 1992, pp. 1986–1992.

[5]Hétu, J.-F., and Pelletier, D., "Fast Adaptive Finite Element Scheme for Viscous Incompressible Flows," *AIAA Journal*, Vol. 30, No. 11, 1992, pp. 2677–2682.

[6]Pelletier, D., and Hétu, J.-F., "An Adaptive Finite Element Methodology for Incompressible Viscous Flows," *Advances in Finite Element Method in Fluid Dynamics, Proceedings of the ASME Winter Annual Meeting* (Anaheim, CA), Nov. 8–13, 1992, pp. 1–12 (FED-137).

[7]Zienkiewicz, O. C., Gago, J. P., and Kelley, D. W., "The Hierarchical Concepts in Finite Element Analysis," *Computers and Structures*, Vol. 16, No. 1, 1983, pp. 53–65.

[8]Lohner, R., Morgan, K., and Zienkiewicz, O. C., "Adaptive Grid Refinement for the Euler and Compressible Navier-Stokes Equations," *Accuracy Estimates and Adaptive Refinement in Finite Element Computations*, edited by I. Babuska, O. C. Zienkiewicz, J. P. Gago, and E. R. de A. Oliveira, Wiley, New York, 1986, pp. 281–298.

[9]Fortin, M., and Fortin, A., "Experiments with Several Elements for Incompressible Flows," *International Journal for Numerical Methods in Fluids*, Vol. 5, No. 9, 1985, pp. 911–928.

[10]Pelletier, D., and Fortin, A., "Are FEM Solutions of Incompressible Flows Really Incompressible? (or how simple flows can cause headaches)," *International Journal for Numerical Methods in Fluids*, Vol. 9, No. 1, 1989, pp. 99–112.

[11]Zienkiewicz, O. C., and Zhu, R. J. Z., "A Simple Error Estimator and Adaptive Procedure for Practical Engineering Analysis," *International Journal for Numerical Methods in Engineering*, Vol. 24, No. 2, 1987, pp. 337–357.

[12]Verfurth, R., "A Posteriori Error Estimate for the Stokes Equations," *Numerishe Mathematik*, Vol. 55, No. 4, 1989, pp. 309–325.

[13]Chen, K. S., Ku, A. C., and Chou, C. H., "Investigation of Natural Convection in Partially Divided Rectangular Enclosure both With and Without an Opening in the Partition Plate: Measurements Results," *Journal of Heat Transfer*, Vol. 112, No. 3, 1990, pp. 648–652.